

---

# HRSAM: Efficiently Segment Anything in High-Resolution Images

---

You Huang, Wenbin Lai, Jiayi Ji, Liujuan Cao\*, Shengchuan Zhang, Rongrong Ji  
Key Laboratory of Multimedia Trusted Perception and Efficient Computing,  
Ministry of Education of China, Xiamen University

## Abstract

The Segment Anything Model (SAM) has significantly advanced interactive segmentation but struggles with high-resolution images crucial for **high-precision** segmentation. This is primarily due to the quadratic space complexity of SAM-implemented attention and the length extrapolation issue in common global attention. This study proposes HRSAM that integrates Flash Attention and incorporates Plain, Shifted and newly proposed Cycle-scan Window (PSCWin) attention to address these issues. The shifted window attention is redesigned with padding to maintain consistent window sizes, enabling effective length extrapolation. The cycle-scan window attention adopts the recently developed State Space Models (SSMs) to ensure global information exchange with minimal computational overhead. Such window-based attention allows HRSAM to perform effective attention computations on scaled input images while maintaining low latency. Moreover, we further propose HRSAM++ that additionally employs a multi-scale strategy to enhance HRSAM’s performance. The experiments on the **high-precision** segmentation datasets HQSeg44K and DAVIS show that high-resolution inputs enable the SAM-distilled HRSAM models to outperform the teacher model while maintaining lower latency. Compared to the SOTAs, HRSAM achieves a 1.56 improvement in interactive segmentation’s NoC95 metric with only 31% of the latency. HRSAM++ further enhances the performance, achieving a 1.63 improvement in NoC95 with just 38% of the latency. Code is available at <https://github.com/YouHuang67/High-Resolution-Segment-Anything.git>.

## 1 Introduction

The Segment Anything Model (SAM) [36] stands as a cornerstone in interactive segmentation [3, 105, 37, 8, 51, 57] and extends its utility to various downstream tasks in computer vision [63, 65, 39, 89, 102, 85]. As an interactive segmentation model, SAM takes simple manual inputs like clicks [31], bounding boxes [36] and coarse masks [37] to predict precise segmentation results, thus reducing the manual labeling costs associated with image segmentation. SAM [36] enhances the overall efficiency of interactive segmentation, setting new benchmarks for speed and performance. Conversely, interactive segmentation serves as a standard for evaluating foundational models [36, 111, 46] on fine-grained visual tasks. This study focuses on mainstream click-based interactive segmentation and further enhances SAM’s performance.

SAM utilizes large Vision Transformers (ViTs) [16, 47] to encode images into embeddings, which are then decoded into segmentation results by a lightweight decoder. Despite SAM’s considerable success, the current implementation of SAM is limited to handling fixed input resolutions of  $1024 \times 1024$ . Nevertheless, real-world applications frequently require visual models to handle high-resolution images, such as those exceeding  $4096 \times 4096$ , which offer richer details and potentially improved

---

\*Corresponding author

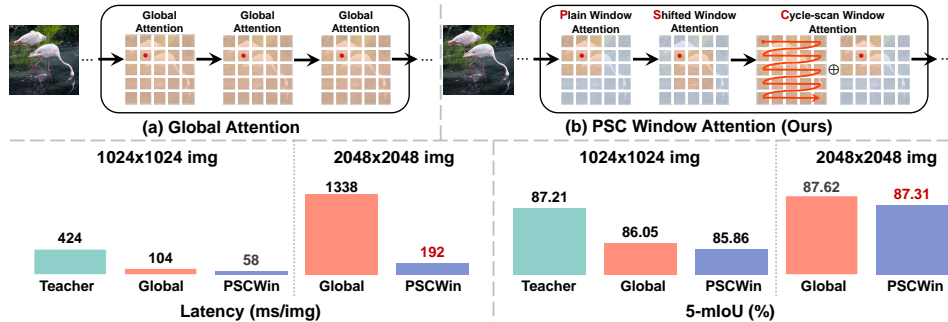


Figure 1: Scalability analysis of global attention and the proposed PSCWin attention. (a) illustrates the global attention, and (b) depicts PSCWin attention. SAM-ViT-Huge is used as the teacher model for distilling into ViTs equipped with either global or PSCWin attention. Latency metrics are determined by the time required to process an image, and segmentation performance is measured by 5-mIoU with five clicks in interactive segmentation over HQSeg44K dataset. Remarkably, the scaled  $2048^2$  resolution enables PSCWin to achieve a 5-mIoU of 87.31% with just 192ms in latency, surpassing the teacher’s 87.21% at 424ms in both performance and speed. Moreover, PSCWin achieves comparable performance to Global Attention with just 14% of the latency in the scaled  $2048^2$  resolution, demonstrating its scalability to large resolutions.

segmentation results. Directly scaling SAM’s input resolution introduces two substantial challenges, *i.e.*, memory inefficiency and lack of scalability to input sizes, which significantly affect performance and efficiency. Firstly, memory inefficiency arises because SAM’s ViTs utilize global attention mechanisms, leading to a quadratic increase in space complexity. Even with  $2048^{22}$  resolution inputs, SAM fails to perform inference on commonly used 3090 GPUs due to insufficient GPU memory. Secondly, the scalability issue becomes apparent. Previous studies indicate that merely increasing the image sizes for SAM cannot proportionally improve performance [78]. This issue originates from the length extrapolation problem [41, 78], where the model’s attention mechanisms struggle to adapt to varying lengths of image token sequences during training and testing, resulting in suboptimal performance given the extensive computational costs for the scaled input image sizes.

To address the above challenges, we introduce HRSAM to harness the performance gains from high-resolution images efficiently. To combat memory inefficiency, we pioneer the integration of Flash Attention [81, 18] within the SAM framework. Flash Attention has been proven across various domains to reduce space complexity from quadratic to linear while maintaining high performance [17, 81]. Notably, the original SAM’s attention mechanism employs relative positional encoding, which is incompatible with Flash Attention. To resolve this, we substitute it with Rotary Position Embedding (RoPE) [80]. Regarding the scalability issue, we incorporate the innovative Plain, Shifted and Cycle-scan Window (PSCWin) attention mechanisms. Plain window attention divides image embeddings into non-overlapping windows, facilitating efficient self-attention. We have modified the vanilla shifted window attention [60, 59] by integrating padding to maintain consistent window sizes. This modification enhances performance during length extrapolation while requiring only a marginal increase in computational resources. Furthermore, our novel cycle-scan window attention marries the newly proposed State Space Models (SSMs) [21] with window attention. SSMs [58, 109] treat image embeddings as sequences, scanning them with approximately linear computational complexity and significantly boosting the efficiency of global information exchange. All the window-based attention mechanisms ensure consistent attention computations throughout both the training and testing phases, thereby addressing length extrapolation problems.

HRSAM further integrates a multi-scale strategy, evolving into HRSAM++, inspired by the successful applications of this strategy [76]. For each image, in addition to resizing to standard resolutions such as  $1024^2$  or  $2048^2$ , we also resize images to a smaller resolution of  $512^2$ . These multi-scale inputs are simultaneously processed by HRSAM++ to analyze image features across different scales with high parallelism. This simultaneous processing is enabled by an indexing operator that efficiently organizes the image embeddings into the proposed PSC windows. In specific blocks, the SSMs [21] are employed for effective multi-scale feature fusion.

<sup>2</sup>In this paper, any resolution expressed as  $N^2$  (e.g.,  $1024^2$ ,  $2048^2$ ,  $3072^2$ ,  $4096^2$ ) refers to an image resolution of  $N \times N$ .

We evaluate HRSAM and HRSAM++ on the high-precision image segmentation datasets HQSeg44K [34] and DAVIS [69]. The results indicate that HRSAM outperforms the previous SOTA by achieving a 1.59% improvement in 5-mIoU while only requiring 31% of the latency. HRSAM++ further sets a new benchmark for high-precision interactive segmentation, delivering SOTA performance with just 38% of the previous SOTA’s latency. Additionally, when distilled solely from SAM-ViT-Huge with low-resolution inputs, without any additional labeled data training, HRSAM models exhibit superior performance with high-resolution inputs while maintaining lower latency than their teacher model. This showcases a cost-effective training strategy for developing high-performance visual foundation models.

Our main contributions are as follows:

- We explore efficient SAM for interactive segmentation to handle high-resolution images. Specifically, we propose HRSAM, utilizing Flash Attention and PSCWin to address memory inefficiency and length extrapolation issues.
- We further propose HRSAM++ that additionally adopts a multi-scale strategy to boost HRSAM’s performance on large-sized input images with slight extra computational costs.
- Our experiments show that HRSAM and HRSAM++ outperform the previous SOTA method in high-precision interactive segmentation with only 31% and 38% of the latency respectively. When merely distilled from SAM with low-resolution inputs, the HRSAMs surpass the teacher in segmentation performance with scaled input sizes while maintaining lower latency.

## 2 Related Work

**Interactive Segmentation.** The integration of deep networks into interactive segmentation begins with DIOS [93], leading to advancements in click-based methods [64, 48, 52, 33, 77]. Subsequent methods focus on enhancing various aspects of interactive segmentation [3, 105, 37, 8, 51, 57, 56, 31, 92, 106, 43, 95, 108, 72, 42]. SAM [36] improves the inference latency by reusing image features, achieving robust zero-shot capabilities and leading to various downstream applications [63, 65, 39, 89, 102, 85, 94, 9]. However, SAM struggles with the high-precision segmentation on high-resolution images, limiting its broader applications. This paper introduces HRSAM to address these issues.

**Efficient Attention.** Attention mechanisms [83] have made significant strides in computer vision [16, 22, 35, 79, 90, 103, 18, 86]. Meanwhile, the high computational complexity of attention mechanisms leads to extensive research on efficient attention [60, 110, 23, 90, 60, 82, 47, 25, 28, 32, 11, 87, 97, 15, 73]. Flash Attention [13, 12] re-implements the vanilla attention mechanism efficiently at the CUDA level, reducing the quadratic space complexity to linear and accelerating computations. This study explores window-based attention to facilitate the attention computations on high-resolution images.

**Visual Length Extrapolation.** Length extrapolation refers to a model’s ability to generalize to longer inputs than those it is trained on [78], which has been explored in NLP [70, 10]. In vision, addressing length extrapolation involves slight modifications of ViTs, e.g., adjustments to positional embeddings and patch sizes [40, 4, 5, 20, 101, 49, 26, 38, 100], and sophisticated training methods, e.g., sequence packing [14] and masking most of image tokens [41]. Recent efforts adapt post-training attention computations to handle scaled input images [78]. Our PSCWin attention achieves scalability to large image size with simple distillation training.

**Visual State Space Model.** Several efforts extend the recently developed State-Space Models (SSMs) [21] to vision, including generation [19, 29, 75], multi-modal tasks [98, 45, 71, 84, 107], medical image analysis [62, 88, 99, 54, 74] and remote sensing [7, 6, 53]. Various studies [109, 58, 44, 96, 30, 61, 68, 67] explore 2D scanning strategies to enhance SSM applications. The proposed cycle-scan in this study simplifies scanning by replicating and concatenating image token sequences.

## 3 Method

This study introduces HRSAM to tackle SAM’s issues of memory inefficiency and length extrapolation on high-resolution images. Section 3.1 provides an overview of HRSAM. Section 3.2 presents both the plain window and the improved shifted window attention. Section 3.3 proposes the cycle-scan window attention. Section 3.4 discusses HRSAM++’s multi-scale strategy.

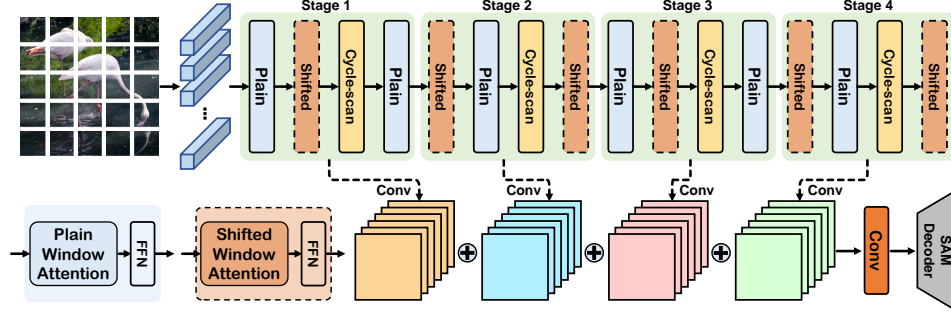


Figure 2: Overview of our proposed HRSAM. HRSAM employs a four-stage encoder with Plain, Shifted and Cycle-scan Window attention blocks. The cycle-scan window block comprises a cycle-scan module and a plain/shifted attention block. These blocks are distributed evenly across the stages. Outputs from all stages are fused through summation and refined via a convolutional block to create final image embeddings fed into the SAM decoder.

### 3.1 Overview of HRSAM

**SAM pipeline.** SAM integrates a heavy ViT-based image encoder, a compact prompt encoder and a light decoder to efficiently generate segmentation results. Prior to interactive segmentation, images are resized to  $H \times W$  (typically  $1024 \times 1024$ ) resolution and undergo offline preprocessing by the image encoder. Such preprocessing produces image embeddings that are repeatedly used in the following steps. During online interaction, the prompt encoder dynamically transforms user prompts such as clicks, bounding boxes and previous segmentation masks into prompt embeddings. The decoder then combines these prompt embeddings with the preprocessed image embeddings to produce the final segmentation results through a series of cross-attention computations. The SAM encoder constitutes  $> 95\%$  of the overall parameters and has a critical impact on the overall performance. Thus, our HRSAM focuses on optimizing the SAM encoder without modifying the other modules.

**HRSAM encoder.** The SAM encoder [36] utilizes ViTs [16] with minor modifications, employing both window-based and global attention in specific blocks [47] and incorporating relative positional encoding during attention computations. Specifically, the SAM-ViT-Base comprises 12 standard transformer blocks, organized into four stages with each stage containing two window-attention blocks and one conventional global-attention block. As depicted in Figure 2, HRSAM also consists of four stages but integrates Plain, Shifted and Cycle-scan Window attention blocks, distributed evenly across each stage. Moreover, HRSAM enhances the encoder by fusing outputs from all four stages through summation, followed by a convolutional block to produce the final  $C$ -dimensional image embeddings  $\mathbf{F} \in \mathbb{R}^{B \times \frac{H}{16} \times \frac{W}{16} \times C}$  ( $B$  is the batch size). Additionally, HRSAM replaces SAM’s relative encoding with RoPE [80] to facilitate the use of Flash Attention [13, 12] since the relative encoding introduces biases in the attention maps that are incompatible with Flash Attention [81, 18].

**Flash Attention.** Flash Attention [13, 12] addresses the memory inefficiency of the conventional attention mechanism [83] by minimizing high-bandwidth memory (HBM) read/write operations. It achieves this through tiling, where attention inputs are processed in smaller, independent blocks, which recalculates the intermedia results when needed instead of accessing HBM. Additionally, Flash Attention utilizes the fast cache, SRAM, with low latency. These collectively reduce memory overhead and transform the attention’s space complexity from quadratic to linear, leading to significant memory efficiency for large-scale attention computations. We provide the details in Appendix A.

**Positional encoding.** SAM’s attention employs the sophisticated relative positional encoding, which hinders the application of Flash Attention [13, 12]. Thus, we replace the encoding with Rotary Position Embedding (RoPE) [80].

### 3.2 Plain and Shifted Window Attention

**Conventional attention.** Given a batch of  $B$  sequentially arranged embedding sets  $\mathbf{X} \in \mathbb{R}^{B \times L \times C}$  with length  $L$ , conventional attention first performs linear projections on  $\mathbf{X}$  to produce the  $Q, K, V \in$

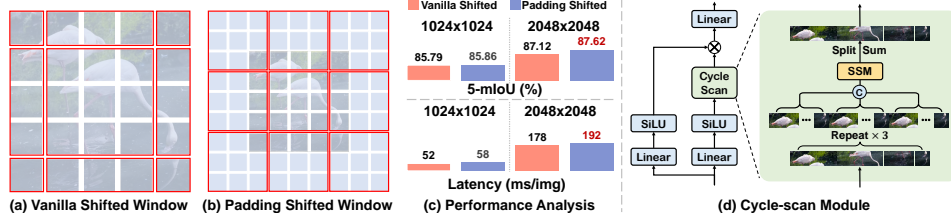


Figure 3: Illustration of proposed padding shifted window and Cycle-scan module.

$\mathbb{R}^{B \times L \times C}$ . Then, the attention outputs are formulated as

$$\text{Attention}(\mathbf{X}) = \text{Linear} \left( \frac{\text{Softmax} \left( \text{Linear}_Q(\mathbf{X}) \text{Linear}_K(\mathbf{X})^\top \right) \text{Linear}_V(\mathbf{X})}{\sqrt{d}} \right), \quad (1)$$

where the matrix multiplication and transpose operators are performed independently for each sample. The discussion of multi-head implementation is omitted since it could be easily extended.

**Plain window attention.** Given the image embeddings  $\mathbf{F} \in \mathbb{R}^{B \times \frac{H}{16} \times \frac{W}{16} \times C}$  and window size  $w$ , the plain window attention [47] firstly rearranges  $\mathbf{F}$  into  $\mathbf{F}_w \in \mathbb{R}^{\frac{BHW}{16^2 w^2} \times w^2 \times C}$ , and then performs the conventional attention, i.e.,  $\text{Attention}(\mathbf{F}_w)$ , which is finally rearranged into the original shape.

**Vanilla shifted window attention.** As depicted in Figure 3 (a), the vanilla shifted window attention introduced in the Swin Transformer [60, 59] shifts the embedding windows to enable interactions across neighboring windows. This process involves moving each embedding within  $\mathbf{F}$  along the x-y axes by a predetermined number of units, with boundary embeddings wrapping around to the opposite side to maintain the dimensions of  $\mathbf{F}$ . This design facilitates more dynamic receptive fields and connectivity between adjacent windows, enhancing the window attention’s ability to integrate contextual information across the entire image.

**Padding shifted window attention.** However, the vanilla shifted window leads to inconsistent window sizes across the embedding windows. To address this, we introduce a padding strategy as depicted in Figure 3 (b). This padding strategy utilizes a learnable embedding  $\mathbf{p} \in \mathbb{R}^C$  to add padding around  $\mathbf{F}$ , ensuring uniform window sizes throughout. Specifically, when applying the vanilla shifting strategy, i.e., shifting  $\mathbf{F}$  along the x-axis by  $S_x$  units and along the y-axis by  $S_y$  units, the proposed padding shifted window instead performs padding of  $w - S_x$  units on the left side along the x-axis and  $w - S_y$  units on the top side along the y-axis. Additional padding is applied to the opposite sides as necessary to ensure a complete number of windows. Although this padding strategy increases the size of  $\mathbf{F}$ , we reduce computational overhead through the replication operator. Before performing the padding,  $\mathbf{F}$  and the learnable padding embedding  $\mathbf{p}$  are both projected through the attention’s QKV-linear layer. Then, the  $(Q, K, V)$  of  $\mathbf{p}$  are replicated and concatenated to the  $(Q, K, V)$  of  $\mathbf{F}$ . After the attention computation, the paddings are discarded, retaining only the region corresponding to  $\mathbf{F}$ . The efficiency and performance impacts of such a padding strategy are detailed in Figure 3 (c).

### 3.3 Cycle-scan Window Attention

**State Space Models.** Structured State Space Models (SSMs) [21] are a class of sequence models designed for sequence-to-sequence transformation, adept at capturing long dependencies among sequential tokens. Specifically, SSMs map a one-dimensional sequence  $x(t) \in \mathbb{R}$  to  $y(t) \in \mathbb{R}$  through an intermediate latent state  $h(t) \in \mathbb{R}^N$ , formulated as:

$$\begin{aligned} h'(t) &= \mathbf{A}h(t) + \mathbf{B}x(t), \\ y(t) &= \mathbf{C}h(t), \end{aligned} \quad (2)$$

where the matrices  $\mathbf{A} \in \mathbb{R}^{N \times N}$ ,  $\mathbf{B} \in \mathbb{R}^{N \times 1}$  and  $\mathbf{C} \in \mathbb{R}^{1 \times N}$  are predefined. Actually, the SSMs are discretized through a zero-order hold rule with a given sample timescale  $\Delta \in \mathbb{R}$ , formulated as

$$\bar{\mathbf{A}} = e^{\Delta \mathbf{A}}, \quad \bar{\mathbf{B}} = (\Delta \mathbf{A})^{-1} (e^{\Delta \mathbf{A}} - \mathbf{I}) \Delta \mathbf{B}, \quad \bar{\mathbf{C}} = \mathbf{C}, \quad (3)$$

which implies the following iterative process:

$$\begin{aligned} h_t &= \bar{\mathbf{A}}h_{t-1} + \bar{\mathbf{B}}x_t, \\ y_t &= \bar{\mathbf{C}}h_t, \end{aligned} \quad (4)$$

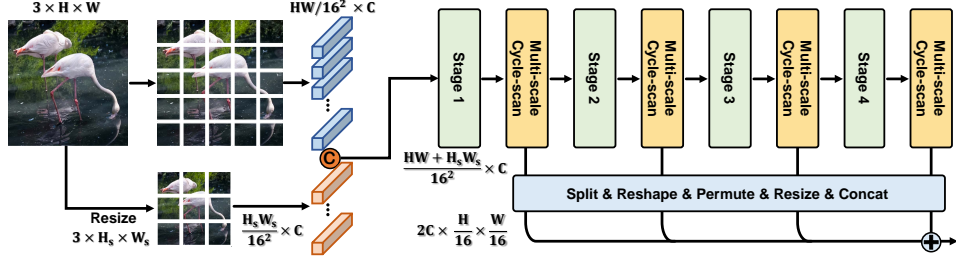


Figure 4: Overview of HRSAM++. HRSAM++ is a multi-scale version of HRSAM that takes both the original and downsampled images as inputs. Multi-scale features are fused at the end of each stage through the multi-scale cycle-scan module. The outputs of these modules are then split by the input scale, resized to a fixed size, and concatenated to form the final output.

where  $1 \leq t \leq L$ . To maintain the efficiency of parallel computation, these iterative steps are transformed into a global convolutional operation:

$$\mathbf{y} = \mathbf{x} * \bar{\mathbf{K}}, \text{ with } \bar{\mathbf{K}} = (\bar{\mathbf{C}}\bar{\mathbf{B}}, \bar{\mathbf{C}}\bar{\mathbf{A}}\bar{\mathbf{B}}, \dots, \bar{\mathbf{C}}\bar{\mathbf{A}}^{L-1}\bar{\mathbf{B}}), \quad (5)$$

where  $*$  is the convolution operation. In summary, the SSM operator takes the input sequence  $\mathbf{x} = \{x_t\}_{t=1}^L$  as inputs, and produces outputs of the same dimension,  $\mathbf{y} = \{y_t\}_{t=1}^L$ . SSMs are capable of modeling global information with linear computational complexity. Additionally, SSMs can be readily extended to handle  $d$ -dimensional sequences  $\mathbf{X} \in \mathbb{R}^{d \times L}$ , processing each channel independently. In this study, we leverage the recent advancements in selective SSMs, specifically the Mamba [21]. For a comprehensive understanding of Mamba, we refer readers to the detailed descriptions available in [21].

**Cycle-scan module.** Mamba’s SSM operator has been employed to scan images from multiple directions to establish spatial dependencies among image tokens [58]. Instead of using sophisticated scanning strategies, we introduce the cycle-scan strategy that simplifies the scanning process by expanding the image token sequence through replication. As illustrated in Figure 3 (d), the proposed cycle-scan strategy repeats the image token sequence three times and connects them sequentially. The Mamba SSM operator then scans the tokens in this order. After scanning, the results are split into the corresponding three sequences and are subsequently merged through summation.

**Cycle-scan window attention.** The cycle-scan module is uniformly integrated into all four stages of the HRSAM, as depicted in Figure 2. Specifically, the scanning is conducted prior to the final block of each stage to facilitate global information exchange among image tokens. The combination of the cycle-scan with either plain or shifted window attention forms the cycle-scan window attention.

### 3.4 Multi-scale Fusion

**Multi-scale inputs.** Multi-scale strategies have been extensively explored in visual tasks due to the proven effectiveness [76]. In this study, we propose a specific multi-scale strategy to address the issue of length extrapolation. This strategy involves resizing any image to a fixed size (e.g.,  $512^2$ ), which provides an overview of the entire scene. Such overview enhances the model’s global understanding and alleviates the issues posed by variable receptive fields across different input sizes. Thus, we further propose an enhanced version of our model, the HRSAM++, which incorporates the additional downsampled input image as depicted in Figure 4. Both the original and additional images are processed concurrently. Multi-scale features from these images are integrated at the end of each stage in the HRSAM++. Further details are discussed subsequently.

**Multi-scale attention.** In HRSAM++, each attention operator is replaced by a multi-scale version, which is facilitated through the block-diagonal mask from Flash Attention [13, 12], enabling parallel processing of multi-scaled inputs. Specifically, both the original  $H \times W$  image and the downsampled  $H_s \times W_s$  image are patchified and concatenated to form a sequence of image tokens with a length of  $(HW + H_sW_s)/16^2$ , as illustrated in Figure 4. During the window attention computations, this token sequence is reorganized by indexing to ensure tokens within the same window are sequential and tokens from the same scale remain contiguous. This reorganization enables the use of Flash Attention for attention computation across the entire token sequence, utilizing the block-diagonal mask to skip unnecessary cross-window attention. This implementation is more efficient and computationally

equivalent to performing attention on isolated windows. Additionally, for padding shifted windows, the learnable padding embedding is firstly appended at the sequence’s end. Then, this padded sequence is similarly reorganized with appropriate token duplication, to maintain size consistency of the windows and undergo the same attention processing. We provide the details in Appendix B C.

**Multi-scale cycle-scan module.** For multi-scale inputs, the cycle-scan module operates in two modes with subtle differences. As shown in Figure 4, HRSAM++ extends the four stages of HRSAM by incorporating an additional multi-scale cycle-scan module, while retaining the original cycle-scan as a single-scale operation within each stage. Both the single and multi-scale cycle-scan modules follow the same process, differing only in the SSMs. The single-scale cycle-scan first splits the tokens by scale, scan each scale’s tokens separately by the SSM, and then concatenates them for post-computation. In contrast, the multi-scale cycle-scan directly performs the SSM across the tokens from all the scales, facilitating the multi-scale fusion.

## 4 Experiments

Section 4.1 details the experimental setup. Section 4.2 discusses the main results. Section 4.3 evaluate HRSAM’s scalability to input sizes. Section 4.4 provides the ablation study of HRSAM’s modules. Section 4.5 presents the qualitative results.

### 4.1 Experimental Setting

We provide the details in Appendix D and the `code` in the supplementary materials.

**Datasets.** We adopt COCO [50], LVIS [24] and HQSeg44K [34] datasets for our two-stage training process. In the first stage, we use only the images from COCO and LVIS without labels, which differs from previous interactive segmentation methods [8, 57, 56, 31]. In the second stage, we finetune the weights pretrained at the first stage using the HQSeg44K training dataset. For testing, we evaluate exclusively on the HQSeg44K validation [34] and DAVIS [69] datasets, both of which have high-precision annotations, following recent advances in high-precision interactive segmentation [55].

**Training strategy.** HRSAM and HRSAM++ undergo the same two-stage training process. In the first stage, we use images from the COCO and LVIS datasets without labels. We employ the vanilla MSE as the loss in the SAM distillation, and minimize the MSE between HRSAM and the teacher’s image embeddings. In the second stage, we further finetune the models using HQSeg44K training samples with segmentation annotations, employing the commonly used normalized focal loss [8, 57, 56, 31].

**Evaluation.** We evaluate HRSAMs against previous methods [37, 8, 56, 31, 55, 36, 104, 91]. In testing, click simulation places clicks at the centers of erroneously predicted regions, aligning with the previous methods [8, 56, 31]. We assess all models’ segmentation performance and speed. Segmentation performance is measured using 5-mIoU and NoC metrics. The 5-mIoU represents the average IoU after the fifth click. The NoC metric indicates the average minimum clicks required to reach a specified IoU. We focus on NoC@90 and NoC@95 within 20 clicks. Speed is quantified as Seconds Per Click (SPC) on GPUs, measuring the average inference latency per click, averaged over 20 clicks. For SAM series models, this includes the preprocessing time by the backbones.

### 4.2 Main Results

As shown in Table 1, when the HRSAM and HRSAM++ are trained by SAM-distillation on  $1024^2$  inputs, scaling the testing input to  $2048^2$  allows them to surpass their teacher SAM-ViT-Huge in performance while retaining a significant speed advantage. These results highlight the scalability of our HRSAM models with respect to input size. Moreover, the further HQ-finetuned HRSAM++ achieves state-of-the-art performance on the high-precision segmentation datasets HQSeg44K and DAVIS, while maintaining a faster SPC latency compared to the previous state-of-the-art SegNext.

### 4.3 Scale Analysis

To analyze the scalability of HRSAM with increased input sizes, we evaluate both HRSAM and HRSAM++ using input sizes of  $1024^2$ ,  $2048^2$ ,  $3072^2$  and  $4096^2$ . The performance of the models are tested on the HQSeg44K dataset, focusing on NoC@90 and NoC@95 metrics. As shown in



Model	Training Data	Latency ↓ 20-SPC (ms)	HQSeg44K <sub>Max HW &gt; 4000</sub>			DAVIS <sub>Max HW &lt; 1000</sub>		
			5-mIoU ↑	NoC90 ↓	NoC95 ↓	5-mIoU ↑	NoC90 ↓	NoC95 ↓
RITM-HRNet32 <sub>400</sub> [37]	COCO+LVIS	46	77.72	10.01	14.58	89.75	5.34	11.45
FocalClick-SegF-B3-S2 <sub>256</sub> [8]	COCO+LVIS	24	84.63	8.12	12.63	90.82	5.17	11.42
FocalClick-SegF-B3-S2 <sub>384</sub> [8]	COCO+LVIS	26	85.45	7.03	10.74	91.22	4.90	10.40
SimpleClick-ViT-B <sub>448</sub> [56]	COCO+LVIS	31	85.11	7.47	12.39	90.73	5.06	10.37
InterFormer-ViT-B <sub>1024</sub> [31]	COCO+LVIS	13	82.62	7.17	10.77	87.79	5.45	11.88
SAM-ViT-B <sub>1024</sub> [36]	SA-1B	12	86.16	7.46	12.42	90.95	5.14	10.74
MobileSAM-ViT-T <sub>1024</sub> [104]	SA-1B	8	81.98	8.70	13.83	89.18	5.83	12.74
EfficientSAM-ViT-T <sub>1024</sub> [91]	ImageNet+SA-1B	6	77.90	10.11	14.60	85.26	7.37	14.28
EfficientSAM-ViT-T <sub>2048</sub> [91]	ImageNet+SA-1B	32	74.20	9.47	13.13	84.10	8.00	14.37
EfficientSAM-ViT-S <sub>1024</sub> [91]	ImageNet+SA-1B	7	79.01	8.84	13.18	87.55	6.37	12.26
EfficientSAM-ViT-S <sub>2048</sub> [91]	ImageNet+SA-1B	60	74.91	8.27	11.97	85.17	6.86	12.49
SegNext (SA×1) ViT-B <sub>1024</sub> [55]	COCO+LVIS	42	85.41	7.47	11.94	90.13	5.46	13.31
SegNext (SA×2) ViT-B <sub>1024</sub> [55]	COCO+LVIS	58	85.71	7.18	11.52	89.85	5.34	12.80
SAM-ViT-H <sub>1024</sub> (Teacher) [36]	SA-1B	29	87.21	6.85	11.57	90.82	5.20	10.04
HRSAM-ViT-B <sub>1024</sub> (Ours)	†COCO+LVIS <sub>w/o labs</sub>	10	85.86	7.66	12.54	89.54	5.48	11.61
HRSAM-ViT-B <sub>2048</sub> (Ours)	†COCO+LVIS <sub>w/o labs</sub>	18	87.31	6.76	11.17	90.36	5.39	10.15
HRSAM <sup>++</sup> -ViT-B <sub>1024</sub> (Ours)	†COCO+LVIS <sub>w/o labs</sub>	12	86.25	7.47	12.33	90.06	5.41	11.35
HRSAM <sup>++</sup> -ViT-B <sub>2048</sub> (Ours)	†COCO+LVIS <sub>w/o labs</sub>	22	88.66	6.11	10.48	90.78	5.08	9.73
<i>Trained on HQSeg44K (HQ)</i>								
HQ-SAM-ViT-B <sub>1024</sub> [63]	SA-1B+HQ	9	89.85	6.49	10.79	91.77	5.26	10.00
SegNext (SA×2) ViT-B <sub>1024</sub> [55]	COCO+LVIS+HQ	58	91.75	5.32	9.42	91.87	4.43	10.73
HRSAM-ViT-B <sub>1024</sub> (Ours)	†COCO+LVIS <sub>w/o labs</sub> +HQ	10	91.81	5.42	9.27	91.34	4.82	11.86
HRSAM-ViT-B <sub>2048</sub> (Ours)	†COCO+LVIS <sub>w/o labs</sub> +HQ	18	<b>93.34</b>	4.37	7.86	92.63	4.22	8.83
HRSAM <sup>++</sup> -ViT-B <sub>1024</sub> (Ours)	†COCO+LVIS <sub>w/o labs</sub> +HQ	12	91.84	5.32	9.18	91.25	5.02	11.64
HRSAM <sup>++</sup> -ViT-B <sub>2048</sub> (Ours)	†COCO+LVIS <sub>w/o labs</sub> +HQ	22	93.32	<b>4.20</b>	<b>7.79</b>	<b>92.73</b>	<b>4.12</b>	<b>8.72</b>

Table 1: Quantitative results. † indicates the model is trained by distillation without using the samples’ labels. Scaling inputs to 2048<sup>2</sup> enables SAM-distilled HRSAM models to surpass their teacher model SAM-ViT-Huge in both performance and speed. The further HQ-finetuned HRSAM<sup>++</sup> achieves state-of-the-art performance on the HQSeg44K and DAVIS datasets, demonstrating superior segmentation performance and faster SPC latency compared to previous SOTA SegNext.

Model	Size (0, 1024]		Size (1024, 2048]		Size (2048, 3072]		Size (3072, 4096]	
	NoC90 ↓	NoC95 ↓	NoC90 ↓	NoC95 ↓	NoC90 ↓	NoC95 ↓	NoC90 ↓	NoC95 ↓
SAM-ViT-H <sub>1024</sub> [36]	5.23	10.27	7.94	13.00	7.67	11.87	7.79	12.45
HRSAM-ViT-B <sub>1024</sub>	5.80	10.99	8.60	13.82	8.19	12.69	9.47	13.25
HRSAM-ViT-B <sub>2048</sub>	<b>5.67</b>	<b>10.16</b>	<b>7.87</b>	<b>12.82</b>	<b>7.08</b>	<b>11.00</b>	<b>7.28</b>	<b>11.56</b>
HRSAM-ViT-B <sub>3072</sub>	6.91	11.24	8.76	13.96	7.75	11.59	7.76	12.24
HRSAM-ViT-B <sub>4096</sub>	8.54	13.25	10.69	15.69	8.99	13.20	8.76	13.56
HRSAM <sup>++</sup> -ViT-B <sub>1024</sub>	5.58	10.78	8.53	13.65	7.97	12.30	9.18	13.19
HRSAM <sup>++</sup> -ViT-B <sub>2048</sub>	<b>4.95</b>	<b>9.42</b>	<b>7.18</b>	<b>12.15</b>	6.46	10.33	6.65	11.14
HRSAM <sup>++</sup> -ViT-B <sub>3072</sub>	5.10	9.87	7.28	12.41	<b>6.27</b>	<b>9.98</b>	<b>6.49</b>	<b>10.74</b>
HRSAM <sup>++</sup> -ViT-B <sub>4096</sub>	5.57	10.82	8.28	13.20	6.36	10.68	6.79	11.33

Table 2: Input size scalability analysis. The metrics NoC@90 and NoC@95 are measured over the HQSeg44K dataset, with differently sized inputs.

Table 2, both HRSAM and HRSAM<sup>++</sup> scale from the 1024<sup>2</sup> training resolution to 2048<sup>2</sup> testing size effectively. However, for larger input sizes, such as 3072<sup>2</sup> and 4096<sup>2</sup>, HRSAM’s performance deteriorates. Even when the images larger than 2048<sup>2</sup> are resized to 3072<sup>2</sup> or 4096<sup>2</sup>, the performance is inferior to resizing to 2048<sup>2</sup>. This decline can be attributed to two main reasons. First, resizing to larger images requires a more robust resizing strategy. The linear interpolation used in this study cannot adequately preserve image details. Second, the models are trained on 1024<sup>2</sup> inputs, but handling inputs larger than 3072<sup>2</sup> involves processing image token sequences more than 9× longer, exceeding the models’ length extrapolation capabilities. On the other hand, HRSAM<sup>++</sup> shows that for larger images (greater than 2048<sup>2</sup>), resizing to 3072<sup>2</sup> can further improve performance, confirming the effectiveness of HRSAM<sup>++</sup>’s multi-scale strategy.

#### 4.4 Ablation Study

In the ablation study, we train HRSAM and its various ablation variants using the same distillation protocol in the main experiments. We analyze the impact of different modules, including Global attention (Global), Plain Window attention (Plain Win), Vanilla Shifted Window attention (Van Swin), Padding Shifted Window attention (Padding Swin), Single-Scale Cycle-scan (SS CScan) and Multi-Scale Cycle-scan (MS CScan). We compare the latency and performance of these variant backbones under 1024<sup>2</sup> and 2048<sup>2</sup> input sizes. As shown in Table 3, the Global attention achieves better performance with 1024<sup>2</sup> inputs due to its strong representation capability, which allows it to



Global	Plain Win	Van Swin	Pad Swin	SS CScan	MS CScan	1024×1024 img			2048×2048 img		
						Lat (ms) ↓	NoC90 ↓	NoC95 ↓	Lat (ms) ↓	NoC90 ↓	NoC95 ↓
✓						104	<b>7.47</b>	<b>12.30</b>	1338	6.89	11.61
✓	✓					61	7.56	12.39	528	6.97	11.57
	✓	✓				37	7.68	12.71	122	6.82	11.44
	✓		✓			44	7.68	12.69	136	6.81	11.36
	✓	✓		✓		52	7.59	12.59	178	6.87	11.34
	✓		✓	✓		58	7.66	12.54	192	6.76	11.17
	✓		✓	✓	✓	98	<b>7.47</b>	12.33	277	<b>6.11</b>	<b>10.48</b>

Table 3: Ablation study of HRSAM’s modules. The modules include Global attention (Global), Plain Window attention (Plain Win), Vanilla Shifted Window attention (Van Swin), Padding Shifted Window attention (Pad Swin), Single-Scale Cycle-scan (SS CScan), and Multi-Scale Cycle-scan (MS CScan). Latency and performance metrics (NoC90 and NoC95) are evaluated under input sizes of  $1024^2$  and  $2048^2$  on HQSeg44K.

effectively learn from the teacher model. However, when scaled to  $2048^2$  inputs, its performance deteriorated significantly compared to other HRSAM variants, with extremely high latency. Conversely, while some HRSAM variants show only moderate performance over  $1024^2$  inputs, they generally perform well when scaled to  $2048^2$ . Notably, HRSAM++ with the Multi-Scale Cycle-scan module demonstrates significant improvements over  $2048^2$  inputs, highlighting the effectiveness of our proposed HRSAM and HRSAM++ in enhancing model scalability to input image sizes.

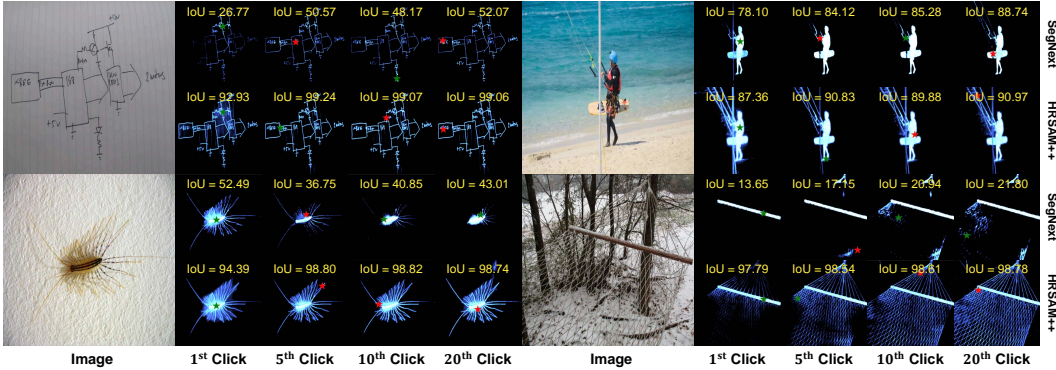


Figure 5: Qualitative comparison of our HRSAM++ and previous SOTA SegNext.

## 4.5 Qualitative Results

In Figure 5, we present a qualitative comparison between our HRSAM++ model and the previous SOTA SegNext [55], using a set of challenging samples with thin edges. We visualize the segmentation results across four different clicks, clearly demonstrating the superior performance of HRSAM++ in high-precision segmentation tasks.

## 5 Limitation

HRSAM cannot scale effectively to excessively large images, as shown in our multi-scale analysis. Over-enlarging input images or processing particularly large images at extremely high resolutions does not improve performance. This presents a challenge in determining the optimal input image size, which HRSAM currently cannot address. Future work will focus on developing adaptive methods to set input sizes more effectively.

## 6 Conclusion

In this paper, we propose HRSAM to address the limitations of SAM in handling high-resolution images critical for high-precision segmentation tasks. HRSAM leverages Flash Attention to resolve the fundamental issue of memory insufficiency on large input images. Then, HRSAM incorporates PSCWin attention ensuring computational consistency during both training and testing. The enhanced version, HRSAM++ additionally adopts a multi-scale strategy. HRSAM models set new benchmarks in high-precision interactive segmentation. Furthermore, our findings reveal a cost-effective training strategy for building high-performance visual foundation models through visual length extrapolation.

## References

- [1] Xformers - flash attention. [https://facebookresearch.github.io/xformers/components/ops.html#xformers.ops.fmha.attn\\_bias.BlockDiagonalMask](https://facebookresearch.github.io/xformers/components/ops.html#xformers.ops.fmha.attn_bias.BlockDiagonalMask). Accessed: 2024-05-18.
- [2] Deconstructing LLM-Flash Attention: A Comprehensive Guide Starting from Softmax. <https://zhuanlan.zhihu.com/p/663932651>, 2023. Accessed: May 21, 2024.
- [3] David Acuna, Huan Ling, Amlan Kar, and Sanja Fidler. Efficient interactive annotation of segmentation datasets with polygon-rnn++. In *2018 IEEE Conference on Computer Vision and Pattern Recognition, CVPR 2018, Salt Lake City, UT, USA, June 18-22, 2018*, pages 859–868. IEEE Computer Society, 2018.
- [4] Lucas Beyer, Pavel Izmailov, Alexander Kolesnikov, Mathilde Caron, Simon Kornblith, Xiaohua Zhai, Matthias Minderer, Michael Tschannen, Ibrahim Alabdulmohsin, and Filip Pavetic. Flexivit: One model for all patch sizes. In *CVPR*, 2023.
- [5] Han Cai, Chuang Gan, Tianzhe Wang, Zhekai Zhang, and Song Han. Once for all: Train one network and specialize it for efficient deployment. *ICLR*, Apr 2020.
- [6] Hongruixuan Chen, Jian Song, Chengxi Han, Junshi Xia, and Naoto Yokoya. Changemamba: Remote sensing change detection with spatio-temporal state space model, 2024.
- [7] Keyan Chen, Bowen Chen, Chenyang Liu, Wenyuan Li, Zhengxia Zou, and Zhenwei Shi. Rsmamba: Remote sensing image classification with state space model, 2024.
- [8] Xi Chen, Zhiyan Zhao, Yilei Zhang, Manni Duan, Donglian Qi, and Hengshuang Zhao. Focalclick: towards practical interactive image segmentation. pages 1300–1309, 2022.
- [9] Junlong Cheng, Jin Ye, Zhongying Deng, Jianpin Chen, Tianbin Li, Haoyu Wang, Yanzhou Su, Ziyang Huang, Jilong Chen, Lei Jiang, et al. Sam-med2d. *arXiv preprint arXiv:2308.16184*, 2023.
- [10] Ta-Chung Chi, Ting-Han Fan, Peter J Ramadge, and Alexander Rudnicky. Kerple: Kernelized relative positional embedding for length extrapolation. *NeurIPS*, 35, 2022.
- [11] Xiangxiang Chu, Zhi Tian, Yuqing Wang, Bo Zhang, Haibing Ren, Xiaolin Wei, Huaxia Xia, and Chunhua Shen. Twins: Revisiting the design of spatial attention in vision transformers. *Neural Information Processing Systems, Neural Information Processing Systems*, Dec 2021.
- [12] Tri Dao. FlashAttention-2: Faster attention with better parallelism and work partitioning. 2023.
- [13] Tri Dao, Daniel Y. Fu, Stefano Ermon, Atri Rudra, and Christopher Ré. FlashAttention: Fast and memory-efficient exact attention with IO-awareness. In *Advances in Neural Information Processing Systems*, 2022.
- [14] Mostafa Dehghani, Basil Mustafa, Josip Djolonga, Jonathan Heek, Matthias Minderer, Mathilde Caron, Andreas Steiner, Joan Puigcerver, Robert Geirhos, Ibrahim Alabdulmohsin, et al. Patch n’pack: Navit, a vision transformer for any aspect ratio and resolution. *arXiv preprint arXiv:2307.06304*, 2023.
- [15] Xiaoyi Dong, Jianmin Bao, Dongdong Chen, Weiming Zhang, Nenghai Yu, Lu Yuan, Dong Chen, and Baining Guo. Cswin transformer: A general vision transformer backbone with cross-shaped windows. In *2022 IEEE/CVF Conference on Computer Vision and Pattern Recognition (CVPR)*, Jun 2022.
- [16] Alexey Dosovitskiy, Lucas Beyer, Alexander Kolesnikov, Dirk Weissenborn, Xiaohua Zhai, Thomas Unterthiner, Mostafa Dehghani, Matthias Minderer, Georg Heigold, Sylvain Gelly, Jakob Uszkoreit, and Neil Houlsby. An image is worth 16x16 words: Transformers for image recognition at scale. In *9th International Conference on Learning Representations, ICLR 2021, Virtual Event, Austria, May 3-7, 2021*. OpenReview.net, 2021.

- [17] Yuxin Fang, Quan Sun, Xinggang Wang, Tiejun Huang, Xinlong Wang, and Yue Cao. Eva-02: A visual representation for neon genesis. *arXiv preprint arXiv:2303.11331*, 2023.
- [18] Yuxin Fang, Wen Wang, Binhui Xie, Quan Sun, Ledell Wu, Xinggang Wang, Tiejun Huang, Xinlong Wang, and Yue Cao. Eva: Exploring the limits of masked visual representation learning at scale. In *Proceedings of the IEEE/CVF Conference on Computer Vision and Pattern Recognition*, pages 19358–19369, 2023.
- [19] Linjie Fu, Xia Li, Xiuding Cai, Yingkai Wang, Xueyao Wang, Yali Shen, and Yu Yao. Md-dose: A diffusion model based on the mamba for radiotherapy dose prediction, 2024.
- [20] Chengyue Gong, Dilin Wang, Meng Li, Xinlei Chen, Zhicheng Yan, Yuandong Tian, Vikas Chandra, et al. Nasvit: Neural architecture search for efficient vision transformers with gradient conflict aware supernet training. In *ICLR*, 2021.
- [21] Albert Gu and Tri Dao. Mamba: Linear-time sequence modeling with selective state spaces. *arXiv preprint arXiv:2312.00752*, 2023.
- [22] Jiaqi Gu, Hyoukjun Kwon, Dilin Wang, Wei Ye, Meng Li, Yu-Hsin Chen, Liangzhen Lai, Vikas Chandra, and David Z Pan. Multi-scale high-resolution vision transformer for semantic segmentation. In *Proceedings of the IEEE/CVF Conference on Computer Vision and Pattern Recognition*, pages 12094–12103, 2022.
- [23] Qipeng Guo, Xipeng Qiu, Pengfei Liu, Yunfan Shao, Xiangyang Xue, and Zheng Zhang. Star-transformer. In *Proceedings of the 2019 Conference of the North*, Jan 2019.
- [24] Agrim Gupta, Piotr Dollár, and Ross B. Girshick. LVIS: A dataset for large vocabulary instance segmentation. In *IEEE Conference on Computer Vision and Pattern Recognition, CVPR 2019, Long Beach, CA, USA, June 16-20, 2019*, pages 5356–5364. Computer Vision Foundation / IEEE, 2019.
- [25] Dongchen Han, Xuran Pan, Yizeng Han, Shiji Song, and Gao Huang. Flatten transformer: Vision transformer using focused linear attention. In *Proceedings of the IEEE/CVF International Conference on Computer Vision*, pages 5961–5971, 2023.
- [26] Kaiming He, Xinlei Chen, Saining Xie, Yanghao Li, Piotr Dollar, and Ross Girshick. Masked autoencoders are scalable vision learners. In *CVPR*, Jun 2022.
- [27] Kaiming He, Georgia Gkioxari, Piotr Dollár, and Ross Girshick. Mask r-cnn. In *Proceedings of the IEEE international conference on computer vision*, pages 2961–2969, 2017.
- [28] Jonathan Ho, Nal Kalchbrenner, Dirk Weissenborn, and Tim Salimans. Axial attention in multidimensional transformers. *Cornell University - arXiv, Cornell University - arXiv*, Sep 2019.
- [29] Vincent Tao Hu, Stefan Andreas Baumann, Ming Gui, Olga Grebenkova, Pingchuan Ma, Johannes Fischer, and Björn Ommer. Zigma: A dit-style zigzag mamba diffusion model, 2024.
- [30] Tao Huang, Xiaohuan Pei, Shan You, Fei Wang, Chen Qian, and Chang Xu. Localmamba: Visual state space model with windowed selective scan, 2024.
- [31] You Huang, Hao Yang, Ke Sun, Shengchuan Zhang, Liujuan Cao, Guannan Jiang, and Rongrong Ji. Interformer: Real-time interactive image segmentation. In *Proceedings of the IEEE/CVF International Conference on Computer Vision*, pages 22301–22311, 2023.
- [32] Zilong Huang, Xinggang Wang, Yunchao Wei, Lichao Huang, Humphrey Shi, Wenyu Liu, and Thomas S. Huang. Ccnet: Criss-cross attention for semantic segmentation. *IEEE Transactions on Pattern Analysis and Machine Intelligence*, page 1–1, Jan 2020.
- [33] Won-Dong Jang and Chang-Su Kim. Interactive image segmentation via backpropagating refinement scheme. In *IEEE Conference on Computer Vision and Pattern Recognition, CVPR 2019, Long Beach, CA, USA, June 16-20, 2019*, pages 5297–5306. Computer Vision Foundation / IEEE, 2019.

- [34] Lei Ke, Mingqiao Ye, Martin Danelljan, Yifan Liu, Yu-Wing Tai, Chi-Keung Tang, and Fisher Yu. Segment anything in high quality. In *NeurIPS*, 2023.
- [35] Salman Khan, Muzammal Naseer, Munawar Hayat, Syed Waqas Zamir, Fahad Shahbaz Khan, and Mubarak Shah. Transformers in vision: A survey. *ACM computing surveys (CSUR)*, 54(10s):1–41, 2022.
- [36] Alexander Kirillov, Eric Mintun, Nikhila Ravi, Hanzi Mao, Chloe Rolland, Laura Gustafson, Tete Xiao, Spencer Whitehead, Alexander C. Berg, Wan-Yen Lo, Piotr Dollár, and Ross Girshick. Segment anything. *arXiv:2304.02643*, 2023.
- [37] Anton Konushin Konstantin Sofiiuk, Ilia A. Petrov. Reviving iterative training with mask guidance for interactive segmentation. *arXiv: Computer Vision and Pattern Recognition*, 2021.
- [38] Aditya Kusupati, Gantavya Bhatt, Aniket Rege, Matthew Wallingford, Aditya Sinha, Vivek Ramanujan, William Howard-Snyder, Kaifeng Chen, Sham Kakade, Prateek Jain, and Ali Farhadi. Matryoshka representations for adaptive deployment. *arXiv preprint arXiv:2205.13147*, May 2022.
- [39] Xin Lai, Zhuotao Tian, Yukang Chen, Yanwei Li, Yuhui Yuan, Shu Liu, and Jiaya Jia. Lisa: Reasoning segmentation via large language model. *arXiv preprint arXiv:2308.00692*, 2023.
- [40] Kenton Lee, Mandar Joshi, Iulia Raluca Turc, Hexiang Hu, Fangyu Liu, Julian Martin Eisen-schlos, Urvashi Khandelwal, Peter Shaw, Ming-Wei Chang, and Kristina Toutanova. Pix2struct: Screenshot parsing as pretraining for visual language understanding. In *ICML*, 2023.
- [41] Vincent Leroy, Jerome Revaud, Thomas Lucas, and Philippe Weinzaepfel. Win-win: Training high-resolution vision transformers from two windows. *arXiv preprint arXiv:2310.00632*, 2023.
- [42] Kehan Li, Yian Zhao, Zhennan Wang, Zesen Cheng, Peng Jin, Xiangyang Ji, Li Yuan, Chang Liu, and Jie Chen. Multi-granularity interaction simulation for unsupervised interactive segmentation. In *Proceedings of the IEEE/CVF International Conference on Computer Vision*, pages 666–676, 2023.
- [43] Kun Li, George Vosselman, and Michael Ying Yang. Interactive image segmentation with cross-modality vision transformers. In *Proceedings of the IEEE/CVF International Conference on Computer Vision*, pages 762–772, 2023.
- [44] Shufan Li, Harkanwar Singh, and Aditya Grover. Mamba-nd: Selective state space modeling for multi-dimensional data, 2024.
- [45] Wenrui Li, Xiaopeng Hong, and Xiaopeng Fan. Spikemba: Multi-modal spiking saliency mamba for temporal video grounding, 2024.
- [46] Xiangtai Li, Haobo Yuan, Wei Li, Henghui Ding, Size Wu, Wenwei Zhang, Yining Li, Kai Chen, and Chen Change Loy. Omg-seg: Is one model good enough for all segmentation? In *CVPR*, 2024.
- [47] Yanghao Li, Hanzi Mao, Ross Girshick, and Kaiming He. Exploring plain vision transformer backbones for object detection.
- [48] Zhuwen Li, Qifeng Chen, and Vladlen Koltun. Interactive image segmentation with latent diversity. In *2018 IEEE Conference on Computer Vision and Pattern Recognition, CVPR 2018, Salt Lake City, UT, USA, June 18-22, 2018*, pages 577–585. IEEE Computer Society, 2018.
- [49] Mingbao Lin, Mengzhao Chen, Yuxin Zhang, Ke Li, Yunhang Shen, Chunhua Shen, and Rongrong Ji. Super vision transformer. *IJCV*, May 2022.
- [50] Tsung-Yi Lin, Michael Maire, Serge Belongie, James Hays, Pietro Perona, Deva Ramanan, Piotr Dollár, and C. Lawrence Zitnick. Microsoft coco: Common objects in context. *Lecture Notes in Computer Science*, 2014.
- [51] Zheng Lin, Zheng-Peng Duan, Zhao Zhang, Chun-Le Guo, and Ming-Ming Cheng. Focuscut: Diving into a focus view in interactive segmentation. pages 2637–2646, 2022.

- [52] Zheng Lin, Zhao Zhang, Lin-Zhuo Chen, Ming-Ming Cheng, and Shao-Ping Lu. Interactive image segmentation with first click attention. In *2020 IEEE/CVF Conference on Computer Vision and Pattern Recognition, CVPR 2020, Seattle, WA, USA, June 13-19, 2020*, pages 13336–13345. IEEE, 2020.
- [53] Chenyang Liu, Keyan Chen, Bowen Chen, Haotian Zhang, Zhengxia Zou, and Zhenwei Shi. Rscama: Remote sensing image change captioning with state space model, 2024.
- [54] Jiarun Liu, Hao Yang, Hong-Yu Zhou, Yan Xi, Lequan Yu, Yizhou Yu, Yong Liang, Guangming Shi, Shaoting Zhang, Hairong Zheng, and Shanshan Wang. Swin-umamba: Mamba-based unet with imagenet-based pretraining, 2024.
- [55] Qin Liu, Jaemin Cho, Mohit Bansal, and Marc Niethammer. Rethinking interactive image segmentation with low latency, high quality, and diverse prompts. *arXiv preprint arXiv:2404.00741*, 2024.
- [56] Qin Liu, Zhenlin Xu, Gedas Bertasius, and Marc Niethammer. Simpleclick: Interactive image segmentation with simple vision transformers. *arXiv preprint arXiv:2210.11006*, 2022.
- [57] Qin Liu, Meng Zheng, Benjamin Planche, Srikrishna Karanam, Terrence Chen, Marc Niethammer, and Ziyang Wu. Pseudoclick: Interactive image segmentation with click imitation. pages 728–745, 2022.
- [58] Yue Liu, Yunjie Tian, Yuzhong Zhao, Hongtian Yu, Lingxi Xie, Yaowei Wang, Qixiang Ye, and Yunfan Liu. Vmamba: Visual state space model. *arXiv preprint arXiv:2401.10166*, 2024.
- [59] Ze Liu, Han Hu, Yutong Lin, Zhuliang Yao, Zhenda Xie, Yixuan Wei, Jia Ning, Yue Cao, Zheng Zhang, Li Dong, et al. Swin transformer v2: Scaling up capacity and resolution. In *Proceedings of the IEEE/CVF conference on computer vision and pattern recognition*, pages 12009–12019, 2022.
- [60] Ze Liu, Yutong Lin, Yue Cao, Han Hu, Yixuan Wei, Zheng Zhang, Stephen Lin, and Baining Guo. Swin transformer: Hierarchical vision transformer using shifted windows. In *Proceedings of the IEEE/CVF international conference on computer vision*, pages 10012–10022, 2021.
- [61] Shaocong Long, Qianyu Zhou, Xiangtai Li, Xuequan Lu, Chenhao Ying, Yuan Luo, Lizhuang Ma, and Shuicheng Yan. Dgmamba: Domain generalization via generalized state space model, 2024.
- [62] Jun Ma, Feifei Li, and Bo Wang. U-mamba: Enhancing long-range dependency for biomedical image segmentation, 2024.
- [63] Jun Ma and Bo Wang. Segment anything in medical images. *arXiv preprint arXiv:2304.12306*, 2023.
- [64] Kevis-Kokitsi Maninis, Sergi Caelles, Jordi Pont-Tuset, and Luc Van Gool. Deep extreme cut: From extreme points to object segmentation. In *2018 IEEE Conference on Computer Vision and Pattern Recognition, CVPR 2018, Salt Lake City, UT, USA, June 18-22, 2018*, pages 616–625. IEEE Computer Society, 2018.
- [65] Maciej A Mazurowski, Haoyu Dong, Hanxue Gu, Jichen Yang, Nicholas Konz, and Yixin Zhang. Segment anything model for medical image analysis: an experimental study. *Medical Image Analysis*, 89:102918, 2023.
- [66] Maxim Milakov and Natalia Gimelshein. Online normalizer calculation for softmax. *arXiv preprint arXiv:1805.02867*, 2018.
- [67] Badri N. Patro and Vijay S. Agneeswaran. Simba: Simplified mamba-based architecture for vision and multivariate time series, 2024.
- [68] Xiaohuan Pei, Tao Huang, and Chang Xu. Efficientvmamba: Atrous selective scan for light weight visual mamba, 2024.

- [69] Federico Perazzi, Jordi Pont-Tuset, Brian McWilliams, Luc Van Gool, Markus H. Gross, and Alexander Sorkine-Hornung. A benchmark dataset and evaluation methodology for video object segmentation. In *2016 IEEE Conference on Computer Vision and Pattern Recognition, CVPR 2016, Las Vegas, NV, USA, June 27-30, 2016*, pages 724–732. IEEE Computer Society, 2016.
- [70] Ofir Press, Noah A Smith, Mike Lewis, et al. Train short, test long: Attention with linear biases enables input length extrapolation. *arXiv preprint arXiv:2108.12409*, 2021.
- [71] Yanyuan Qiao, Zheng Yu, Longteng Guo, Sihan Chen, Zijia Zhao, Mingzhen Sun, Qi Wu, and Jing Liu. VI-mamba: Exploring state space models for multimodal learning, 2024.
- [72] Amit Kumar Rana, Sabarinath Mahadevan, Alexander Hermans, and Bastian Leibe. Dynamite: Dynamic query bootstrapping for multi-object interactive segmentation transformer. In *Proceedings of the IEEE/CVF International Conference on Computer Vision*, pages 1043–1052, 2023.
- [73] Pengzhen Ren, Changlin Li, Guangrun Wang, Yun Xiao, and QingDuXiaodanLiangXiaoJun Chang. Beyond fixation: Dynamic window visual transformer.
- [74] Jiacheng Ruan and Suncheng Xiang. Vm-unet: Vision mamba unet for medical image segmentation, 2024.
- [75] Qihong Shen, Xuanyu Yi, Zike Wu, Pan Zhou, Hanwang Zhang, Shuicheng Yan, and Xinchao Wang. Gamba: Marry gaussian splatting with mamba for single view 3d reconstruction, 2024.
- [76] Baifeng Shi, Ziyang Wu, Maolin Mao, Xin Wang, and Trevor Darrell. When do we not need larger vision models? *arXiv preprint arXiv:2403.13043*, 2024.
- [77] Konstantin Sofiiuk, Ilia A. Petrov, Olga Barinova, and Anton Konushin. F-BRS: rethinking backpropagating refinement for interactive segmentation. In *2020 IEEE/CVF Conference on Computer Vision and Pattern Recognition, CVPR 2020, Seattle, WA, USA, June 13-19, 2020*, pages 8620–8629. IEEE, 2020.
- [78] Yiran Song, Qianyu Zhou, Xiangtai Li, Deng-Ping Fan, Xuequan Lu, and Lizhuang Ma. Ba-sam: Scalable bias-mode attention mask for segment anything model. *arXiv preprint arXiv:2401.02317*, 2024.
- [79] Robin Strudel, Ricardo Garcia, Ivan Laptev, and Cordelia Schmid. Segmenter: Transformer for semantic segmentation. pages 7262–7272, 2021.
- [80] Jianlin Su, Murtadha Ahmed, Yu Lu, Shengfeng Pan, Wen Bo, and Yunfeng Liu. Roformer: Enhanced transformer with rotary position embedding. *Neurocomputing*, 568:127063, 2024.
- [81] Hugo Touvron, Thibaut Lavril, Gautier Izacard, Xavier Martinet, Marie-Anne Lachaux, Timothée Lacroix, Baptiste Rozière, Naman Goyal, Eric Hambro, Faisal Azhar, et al. Llama: Open and efficient foundation language models. *arXiv preprint arXiv:2302.13971*, 2023.
- [82] Ashish Vaswani, Prajit Ramachandran, Aravind Srinivas, Niki Parmar, Blake Hechtman, and Jonathon Shlens. Scaling local self-attention for parameter efficient visual backbones. In *2021 IEEE/CVF Conference on Computer Vision and Pattern Recognition (CVPR)*, Jun 2021.
- [83] Ashish Vaswani, Noam Shazeer, Niki Parmar, Jakob Uszkoreit, Llion Jones, Aidan N. Gomez, Lukasz Kaiser, and Illia Polosukhin. Attention is all you need. In Isabelle Guyon, Ulrike von Luxburg, Samy Bengio, Hanna M. Wallach, Rob Fergus, S. V. N. Vishwanathan, and Roman Garnett, editors, *Advances in Neural Information Processing Systems 30: Annual Conference on Neural Information Processing Systems 2017, December 4-9, 2017, Long Beach, CA, USA*, pages 5998–6008, 2017.
- [84] Zifu Wan, Yuhao Wang, Silong Yong, Pingping Zhang, Simon Stepputtis, Katia Sycara, and Yaqi Xie. Sigma: Siamese mamba network for multi-modal semantic segmentation, 2024.
- [85] Jiaqi Wang, Zhengliang Liu, Lin Zhao, Zihao Wu, Chong Ma, Sigang Yu, Haixing Dai, Qiushi Yang, Yiheng Liu, Songyao Zhang, et al. Review of large vision models and visual prompt engineering. *arXiv preprint arXiv:2307.00855*, 2023.

- [86] Wenhai Wang, Jifeng Dai, Zhe Chen, Zhenhang Huang, Zhiqi Li, Xizhou Zhu, Xiaowei Hu, Tong Lu, Lewei Lu, Hongsheng Li, et al. Internimage: Exploring large-scale vision foundation models with deformable convolutions. In *Proceedings of the IEEE/CVF Conference on Computer Vision and Pattern Recognition*, pages 14408–14419, 2023.
- [87] Wenxiao Wang, Lu Yao, Long Chen, Deng Cai, Xiaofei He, and Wei Liu. Crossformer: A versatile vision transformer based on cross-scale attention. *arXiv: Computer Vision and Pattern Recognition, arXiv: Computer Vision and Pattern Recognition*, Jul 2021.
- [88] Ziyang Wang, Jian-Qing Zheng, Yichi Zhang, Ge Cui, and Lei Li. Mamba-unet: Unet-like pure visual mamba for medical image segmentation, 2024.
- [89] Junde Wu, Rao Fu, Huihui Fang, Yuanpei Liu, Zhaowei Wang, Yanwu Xu, Yueming Jin, and Tal Arbel. Medical sam adapter: Adapting segment anything model for medical image segmentation. *arXiv preprint arXiv:2304.12620*, 2023.
- [90] Enze Xie, Wenhai Wang, Zhiding Yu, Animashree Anandkumar, JoseM. Alvarez, and Ping Luo. Segformer: Simple and efficient design for semantic segmentation with transformers. *Cornell University - arXiv, Cornell University - arXiv*, Dec 2021.
- [91] Yunyang Xiong, Bala Varadarajan, Lemeng Wu, Xiaoyu Xiang, Fanyi Xiao, Chenchen Zhu, Xiaoliang Dai, Dilin Wang, Fei Sun, Forrest Iandola, et al. EfficientSAM: Leveraged masked image pretraining for efficient segment anything. *arXiv preprint arXiv:2312.00863*, 2023.
- [92] Long Xu, Yongquan Chen, Rui Huang, Feng Wu, and Shiwu Lai. Structured click control in transformer-based interactive segmentation. *arXiv preprint arXiv:2405.04009*, 2024.
- [93] Ning Xu, Brian L. Price, Scott Cohen, Jimei Yang, and Thomas S. Huang. Deep interactive object selection. In *2016 IEEE Conference on Computer Vision and Pattern Recognition, CVPR 2016, Las Vegas, NV, USA, June 27-30, 2016*, pages 373–381. IEEE Computer Society, 2016.
- [94] Shilin Xu, Haobo Yuan, Qingyu Shi, Lu Qi, Jingbo Wang, Yibo Yang, Yining Li, Kai Chen, Yunhai Tong, Bernard Ghanem, et al. Rap-sam: Towards real-time all-purpose segment anything. *arXiv preprint arXiv:2401.10228*, 2024.
- [95] Cilin Yan, Haochen Wang, Jie Liu, Xiaolong Jiang, Yao Hu, Xu Tang, Guoliang Kang, and Efstratios Gavves. Piclick: Picking the desired mask in click-based interactive segmentation. *arXiv preprint arXiv:2304.11609*, 2023.
- [96] Chenhongyi Yang, Zehui Chen, Miguel Espinosa, Linus Ericsson, Zhenyu Wang, Jiaming Liu, and Elliot J. Crowley. Plainmamba: Improving non-hierarchical mamba in visual recognition, 2024.
- [97] Jianwei Yang, Chunyuan Li, Pengchuan Zhang, Xiyang Dai, Bin Xiao, Lu Yuan, Jianfeng Gao, MicrosoftResearchAt Redmond, Microsoft Cloud, and + Ai. Focal self-attention for local-global interactions in vision transformers.
- [98] Yuhuan Yang, Chaofan Ma, Jiangchao Yao, Zhun Zhong, Ya Zhang, and Yanfeng Wang. Remamber: Referring image segmentation with mamba twister, 2024.
- [99] Zi Ye, Tianxiang Chen, Fangyijie Wang, Hanwei Zhang, Guanxi Li, and Lijun Zhang. P-mamba: Marrying perona malik diffusion with mamba for efficient pediatric echocardiographic left ventricular segmentation, 2024.
- [100] Hongxu Yin, Arash Vahdat, Jose Alvarez, Arun Mallya, Jan Kautz, and Pavlo Molchanov. Adavit: Adaptive tokens for efficient vision transformer. *arXiv preprint arXiv:2112.07658*, 2021.
- [101] Jiahui Yu, Pengchong Jin, Hanxiao Liu, Gabriel Bender, Pieter-Jan Kindermans, Mingxing Tan, Thomas Huang, Xiaodan Song, Ruoming Pang, and Quoc Le. Bignas: Scaling up neural architecture search with big single-stage models. In *ECCV*, Jan 2020.



- [102] Tao Yu, Runseng Feng, Ruoyu Feng, Jinming Liu, Xin Jin, Wenjun Zeng, and Zhibo Chen. Inpaint anything: Segment anything meets image inpainting. *arXiv preprint arXiv:2304.06790*, 2023.
- [103] Yuhui Yuan, Rao Fu, Lang Huang, Weihong Lin, Chao Zhang, Xilin Chen, and Jingdong Wang. Hrformer: High-resolution vision transformer for dense predict. *Advances in Neural Information Processing Systems*, 34:7281–7293, 2021.
- [104] Chaoning Zhang, Dongshen Han, Yu Qiao, Jung Uk Kim, Sung-Ho Bae, Seungkyu Lee, and Choong Seon Hong. Faster segment anything: Towards lightweight sam for mobile applications. *arXiv preprint arXiv:2306.14289*, 2023.
- [105] Shiyin Zhang, Jun Hao Liew, Yunchao Wei, Shikui Wei, and Yao Zhao. Interactive object segmentation with inside-outside guidance. In *2020 IEEE/CVF Conference on Computer Vision and Pattern Recognition, CVPR 2020, Seattle, WA, USA, June 13-19, 2020*, pages 12231–12241. IEEE, 2020.
- [106] Tiezheng Zhang, Xiaoxi Chen, Chongyu Qu, Alan Yuille, and Zongwei Zhou. Leveraging ai predicted and expert revised annotations in interactive segmentation: Continual tuning or full training? *arXiv preprint arXiv:2402.19423*, 2024.
- [107] Han Zhao, Min Zhang, Wei Zhao, Pengxiang Ding, Siteng Huang, and Donglin Wang. Cobra: Extending mamba to multi-modal large language model for efficient inference, 2024.
- [108] Minghao Zhou, Hong Wang, Qian Zhao, Yuexiang Li, Yawen Huang, Deyu Meng, and Yefeng Zheng. Interactive segmentation as gaussian process classification. In *Proceedings of the IEEE/CVF Conference on Computer Vision and Pattern Recognition*, pages 19488–19497, 2023.
- [109] Lianghui Zhu, Bencheng Liao, Qian Zhang, Xinlong Wang, Wenyu Liu, and Xinggang Wang. Vision mamba: Efficient visual representation learning with bidirectional state space model. *arXiv preprint arXiv:2401.09417*, 2024.
- [110] Shen Zhuoran, Zhang Mingyuan, Zhao Haiyu, Yi Shuai, and Li Hongsheng. Efficient attention: Attention with linear complexities. In *2021 IEEE Winter Conference on Applications of Computer Vision (WACV)*, Jan 2021.
- [111] Xueyan Zou, Jianwei Yang, Hao Zhang, Feng Li, Linjie Li, Jianfeng Wang, Lijuan Wang, Jianfeng Gao, and Yong Jae Lee. Segment everything everywhere all at once. *Advances in Neural Information Processing Systems*, 36, 2024.

## A Flash Attention

The following introduction to Flash Attention [13, 12] is based on [2].

### A.1 Motivation

Flash Attention is motivated by the need to optimize memory bandwidth and computation speed in GPUs, particularly leveraging High Bandwidth Memory (HBM) and Static Random-Access Memory (SRAM). In GPUs like the A100-40GB, HBM provides 40GB of memory with a bandwidth of 1.5TB/s. However, actual GPU computations occur in SRAM, which has a much higher bandwidth of 19TB/s but is limited to only 20MB of usable memory. The substantial speed difference (SRAM being 12.67 times faster than HBM) and the limited SRAM capacity create a bottleneck when memory exchanges between SRAM and HBM are required.

The primary goal of Flash Attention is to minimize memory exchanges between SRAM and HBM during attention computation. Traditional attention mechanisms require seven exchanges between these memory types, creating significant overhead. Flash Attention aims to perform the entire attention computation within the 20MB SRAM, thus avoiding these costly memory swaps and achieving up to a  $7.6\times$  speedup for  $N \times N$  matrix computations.

### A.2 SRAM Cache Overflow Example

To illustrate the efficiency of Flash Attention, consider a scenario where SRAM can handle 10000 data points at a time. For a single vector, let's say Q and K are both of size [100, 100]. Loading both vectors would require  $2 \times 100 \times 100 = 20000$  data points, which exceeds the 10000 data points capacity of SRAM, necessitating write/read operations to HBM.

To address this, Flash Attention splits the vectors into smaller chunks:

- Split  $Q[100, 100]$  into  $\{Q1[50, 100], Q2[50, 100]\}$
- Split  $K[100, 100]$  into  $\{K1[50, 100], K2[50, 100]\}$

This way, the computation of the attention score

$$\text{score}_{ij} = Q_i K_j^T$$

can be completed entirely within SRAM, avoiding the need to swap data with HBM. By processing these smaller chunks within the high-speed SRAM, Flash Attention efficiently computes the attention scores block-wise, thereby maintaining high computational speed and minimizing memory bottlenecks.

In summary, Flash Attention leverages the speed of SRAM by minimizing memory exchanges and efficiently handling data within the limited capacity of SRAM, resulting in significant performance improvements in attention computation. Next, we detail the algorithm of Flash Attention, beginning with the reformulation of attention's softmax operator.

### A.3 Softmax

**Numerically stable softmax.** Before discussing further details of Flash Attention, we reformulate the conventional softmax operator into a numerically stable version as follows:

$$\text{softmax}(x_i) = \frac{\exp(x_i - \max_k x_k)}{\sum_{j=1}^n \exp(x_j - \max_k x_k)}.$$

**Online softmax.** The softmax has a computationally equivalent online version [66], implemented with three-pass as follows:

$$\begin{aligned}
& m_0 \leftarrow -\infty \\
& d_0 \leftarrow 0.0 \\
& \text{for } i \leftarrow 1, N \\
& \quad m_i \leftarrow \max(m_{i-1}, x_i) \\
& \text{for } i \leftarrow 1, N \\
& \quad d_i \leftarrow d_{i-1} + \exp(x_i - m_N) \\
& \text{for } i \leftarrow 1, N \\
& \quad a_i \leftarrow \exp(x_i - m_N) / d_N
\end{aligned}$$

We then reformulate  $d_i$  with the iterative version,  $d'_i$ , defined as

$$\begin{aligned}
d'_i &= \sum_{j=1}^i \exp(x_j - m_i) \\
&= \left( \sum_{j=1}^{i-1} \exp(x_j - m_i) + \exp(x_i - m_i) \right) \\
&= \exp(m_{i-1} - m_i) \left( \sum_{j=1}^{i-1} \exp(x_j - m_{i-1}) \right) + \exp(x_i - m_i) \\
&= \exp(m_{i-1} - m_i) d'_{i-1} + \exp(x_i - m_i),
\end{aligned}$$

which implies the following two-pass implementation of online softmax:

$$\begin{aligned}
& m_0 \leftarrow -\infty \\
& d_0 \leftarrow 0.0 \\
& \text{for } i \leftarrow 1, N \\
& \quad m_i \leftarrow \max(m_{i-1}, x_i) \\
& \quad d'_i \leftarrow \exp(m_{i-1} - m_i) d'_{i-1} + \exp(x_i - m_i) \\
& \text{for } i \leftarrow 1, N \\
& \quad a_i \leftarrow \exp(x_i - m_N) / d_N
\end{aligned}$$

#### A.4 Flash Attention by Online Softmax

**Two-pass Attention.** Based on the two-pass online softmax, we derive a two-pass implementation of attention, with the pre-computed  $Q, K, V \in \mathbb{R}^{N \times d}$ , as follows:

$$\begin{aligned}
& \text{for } i \leftarrow 1, N \\
& \quad x_i \leftarrow Q[k, :] K^T[:, i] \\
& \quad m_i \leftarrow \max(m_{i-1}, x_i) \\
& \quad d'_i \leftarrow \exp(m_{i-1} - m_i) d'_{i-1} + \exp(x_i - m_i) \\
& \text{for } i \leftarrow 1, N \\
& \quad a_i \leftarrow \frac{\exp(x_i - m_N)}{d'_N} \\
& \quad o_i \leftarrow o_{i-1} + a_i V[i, :]
\end{aligned}$$

**Vanilla Flash Attention.** We reformulate the output  $o_i$  as

$$\begin{aligned}
o_i &= o_{i-1} + \frac{\exp(x_i - m_N)}{d'_N} V[i, :] \\
\implies o_i &= \sum_{j=1}^i \frac{\exp(x_j - m_N)}{d'_N} V[j, :],
\end{aligned}$$

which inspires the following definition

$$o'_i = \sum_{j=1}^i \frac{\exp(x_j - m_i)}{d'_i} V[j, :],$$

where  $o_i = o'_i$  holds if  $i = N$ . Then, we rewrite  $o'_i$  in an iterative form:

$$\begin{aligned} o'_i &= \sum_{j=1}^i \frac{\exp(x_j - m_i)}{d'_i} V[j, :] \\ &= \left( \sum_{j=1}^{i-1} \frac{\exp(x_j - m_i)}{d'_i} V[j, :] \right) + \frac{\exp(x_i - m_i)}{d'_i} V[i, :] \\ &= \left( \sum_{j=1}^{i-1} \frac{\exp(x_j - m_{i-1})}{d'_{i-1}} \frac{\exp(x_j - m_i)}{\exp(x_j - m_{i-1})} \frac{d'_{i-1}}{d'_i} V[j, :] \right) + \frac{\exp(x_i - m_i)}{d'_i} V[i, :] \\ &= \left( \sum_{j=1}^{i-1} \frac{\exp(x_j - m_{i-1})}{d'_{i-1}} V[j, :] \right) \frac{\exp(x_j - m_i)}{\exp(x_j - m_{i-1})} \frac{d'_{i-1}}{d'_i} + \frac{\exp(x_i - m_i)}{d'_i} V[i, :] \\ &= \left( \sum_{j=1}^{i-1} \frac{\exp(x_j - m_{i-1})}{d'_{i-1}} V[j, :] \right) \frac{d'_{i-1} \exp(m_{i-1} - m_i)}{d'_i} + \frac{\exp(x_i - m_i)}{d'_i} V[i, :] \\ &= o'_{i-1} \frac{d'_{i-1} \exp(m_{i-1} - m_i)}{d'_i} + \frac{\exp(x_i - m_i)}{d'_i} V[i, :]. \end{aligned}$$

Thus, we derive the one-pass iterative form of Flash Attention:

$$\begin{aligned} &\text{for } i \leftarrow 1, N \\ &\quad x_i \leftarrow Q[k, :] K^T[:, i] \\ &\quad m_i \leftarrow \max(m_{i-1}, x_i) \\ &\quad d'_i \leftarrow d'_{i-1} \exp(m_{i-1} - m_i) + \exp(x_i - m_i) \\ &\quad o'_i \leftarrow o'_{i-1} \frac{d'_{i-1} \exp(m_{i-1} - m_i)}{d'_i} + \frac{\exp(x_i - m_i)}{d'_i} V[i, :] \\ &\text{end} \\ &O[k, :] \leftarrow o'_N \end{aligned}$$

## A.5 Tiling Flash-Attention

When dealing with multiple data tiles, the Flash Attention algorithm can be further refined as follows:

$$\begin{aligned} &\text{for } i \leftarrow 1 \# \text{tiles} \\ &\quad x_i \leftarrow Q[k, :] K^T[:, (i-1)b : ib] \\ &\quad m_i^{\text{local}} \leftarrow \max_{j=1}^b (x_i[j]) \\ &\quad m_i \leftarrow \max(m_{i-1}, m_i^{\text{local}}) \\ &\quad d'_i \leftarrow d'_{i-1} \exp(m_{i-1} - m_i) + \sum_{j=1}^b \exp(x_i[j] - m_i) \\ &\quad o'_i \leftarrow o'_{i-1} \frac{d'_{i-1}}{d'_i} \exp(m_{i-1} - m_i) + \sum_{j=1}^b \frac{\exp(x_i[j] - m_i)}{d'_i} V[j + (i-1)b, :] \\ &\text{end} \\ &O[k, :] \leftarrow o'_N \end{aligned}$$

## A.6 Memory Efficiency of Flash Attention

Based on the above derivation, it can be observed that Flash Attention requires only a fixed amount of memory to execute efficient tiling. Thus, Flash Attention algorithm eliminates the need to store the entire attention map, thereby reducing the quadratic space complexity to linear, primarily for storing computational results.

## A.7 Limitation

As outlined in the derivation process, the transition from online softmax to two-pass softmax and one-pass attention computation heavily relies on sophisticated mathematical derivations and strict formalism. Although Flash Attention optimizes the conventional attention computation process, it is incompatible with certain attention variants, such as the relative positional encoding used in SAM [36]. This type of encoding requires adding an additional attention bias to the attention map, i.e.,  $\text{softmax}(QK^T + \text{bias})V$ , which cannot be integrated into the one-pass attention algorithm of Flash Attention. As a result, SAM cannot directly utilize Flash Attention.

## B Block-diagonal Attention

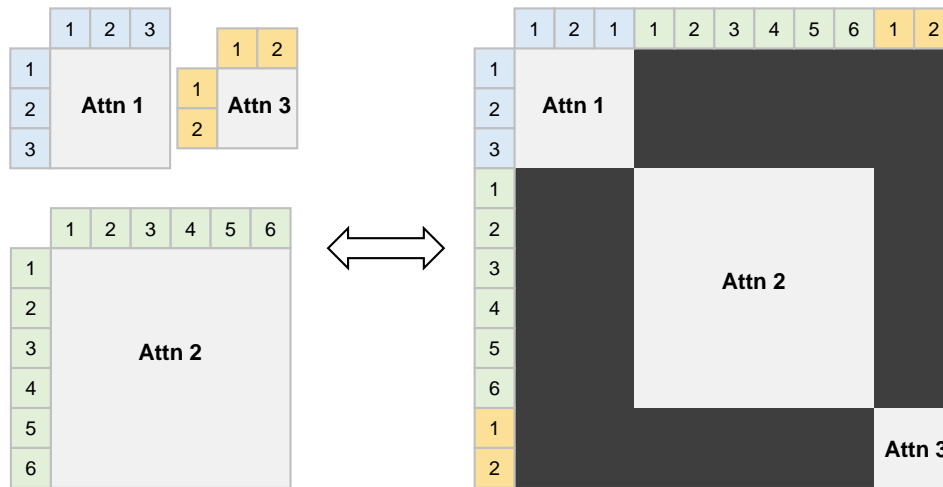


Figure 6: Illustration of block-diagonal attention [1].

Flash Attention supports block-diagonal mode [1] for computing attention. This mode introduces a skip mechanism to the previously discussed one-pass attention algorithm, which skips the ignored parts of the attention map. Consequently, multiple attention computations can be merged using block-diagonal attention.

As shown in Figure 6, multiple token sequences of different lengths can be combined into a single token sequence. By constructing an appropriate mask to block attention between different token sequences, the CUDA implementation of Flash Attention can skip these irrelevant attentions. This takes full advantage of the highly parallel nature of GPUs to process multiple token sequences simultaneously.

Moreover, this strategy can be used for vanilla shifted window attention with differently sized window attentions and is particularly effective for the proposed padding shifted window. By providing the diagonal mask dividing the image tokens into equal-sized windows, we can directly calculate attention without reshaping the image token sequence to construct windows. This method optimizes the computation process, ensuring efficient and simultaneous processing of multiple token sequences. Additionally, the multi-scale image tokens are similarly concatenated and processed by the block-diagonal attention with the attention computed within the same-scale tokens.

## C Indexing Operator

For instance, the multi-scale image token sequence is formulated as the concatenated embeddings  $\mathbf{F}_c = \text{Concat}(\mathbf{F}, \mathbf{F}_s) \in \mathbb{R}^{(L+L_s) \times C}$ , with  $L = \frac{HW}{16^2}$  and  $L_s = \frac{H_s W_s}{16^2}$ . Assume the window size is  $S$ , which is divisible by  $\frac{H}{16}$  and  $\frac{W}{16}$  for simplicity. We then detail the plain and padding shifted window operations over the multi-scale token sequences using the indexing operator.

### C.1 Indexing Multi-scale Plain Window.

The single-scale plain window is created by reshaping  $\mathbf{F}$  to obtain the windowed embeddings  $\mathbf{F}_w \in \mathbb{R}^{\frac{L}{S^2} \times S^2 \times C}$ , where each window  $\mathbf{F}_w[i] \in \mathbb{R}^{S^2 \times C}$  is processed using conventional attention. For the multi-scale plain window,  $\mathbf{F}_c$  is rearranged so that tokens within the same window are contiguous in the sequence, as shown in Figure 7 (a). The block-diagonal attention is then applied to the rearranged sequence with a mask that restricts attention to the local window.

### C.2 Indexing Multi-scale Padding Shifted Window.

Similarly, the multi-scale padding shifted window requires a rearranged token sequence. The difference lies in the additional padding token, as illustrated in Figure 7 (b). This padding token is appended at the end of the token sequence and replicated according to the indices. The same block-diagonal attention is then applied.

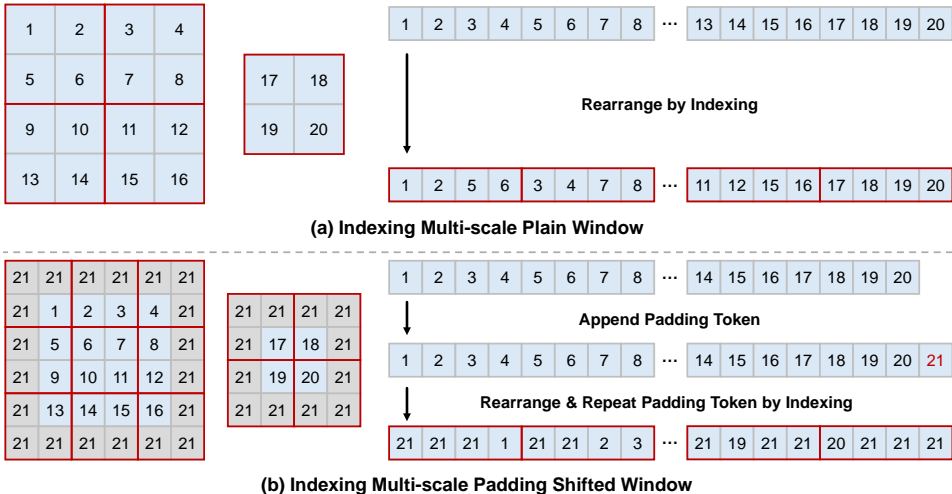


Figure 7: Illustration of the indexing operator. The red boxes in the sequence indicate the regions where self-attention is computed.

## D Experimental Details

### D.1 Datasets.

We adopt COCO [50], LVIS [24] and HQSeg44K [34] datasets for our two-stage training process. Specifically, the COCO dataset includes 118K training images (1.2M instances). LVIS shares the same images as COCO with superior quality of segmentation annotations. HQSeg44K comprises six existing image datasets, including DIS, ThinObject-5K, FSS-1000, ECSSD, MSRA10K and DUT-OMRON, containing extremely high-precision segmentation annotations.

In the first stage, we use only the images from COCO and LVIS without the labels in our distillation training, which differs from previous interactive segmentation methods [8, 57, 56, 31]. In the second stage, we finetune the weights pretrained at the first stage using the HQSeg44K training dataset. For testing, we evaluate exclusively on the HQSeg44K validation [34] and DAVIS [69] datasets, both of which have high-precision annotations, following recent advances in high-precision interactive segmentation [55].

## D.2 Implementation details.

We utilize ViT-Base [16, 27] as the backbone for HRSAM, retaining SAM’s prompt encoder and decoder. The ViT-Base consists of 12 blocks, equally divided into four stages. The cycle-scan module is introduced before the last block of each stage. For the enhanced version, HRSAM++, an additional multi-scale cycle-scan module is inserted at the end of each stage. Similar to the Swin Transformer [60], we alternate between plain window attention and the proposed padding shifted window attention. Each block has an embedding dimension of 768, and the output dimension of each stage is 256, aligning with SAM decoder’s inputs. Besides, we initialize HRSAM-ViT-Base by the MAE-pretrained weights [27], following the previous works [56, 31, 55]. In addition, the typical FFN has a hidden layer dimension of  $768 \times 4$ , with a uniform window size set to 16. The hidden state of Mamba is configured as 32, and the number of attention’s heads is set to 12.

## D.3 Training strategy.

In the training process, we follow a two-stage approach. In the first stage, images from the COCO and LVIS training datasets are used. Initially, the teacher model SAM-ViT-Huge’s backbone is employed to perform inference on these images, and the resulting image embeddings are stored. During HRSAM training, these precomputed embeddings are loaded, and the training images undergo simple color augmentation without other augmentation methods. HRSAM computes its own image embeddings on these augmented images, and the difference between HRSAM and the teacher embeddings is minimized using vanilla MSE as the loss function. In the second stage, we further finetune the models using HQSeg44K training samples with segmentation annotations. We employ the commonly used normalized focal loss for this finetuning stage.

Both stages share most of the training settings. The optimizer is AdamW with weight decay of 0.05 and betas of (0.9, 0.999). We use a learning rate scheduler with a linear warm-up starting from  $1 \times 10^{-6}$  and a polynomial decay starting from  $1 \times 10^{-4}$  over 160k iterations for the first stage and 40k iterations for the second stage. Additionally, during the second stage, we apply additional random flip augmentation to the images. Training is conducted on 4 NVIDIA RTX 3090 GPUs with a batch size of 1 per GPU.

## D.4 Evaluation.

We evaluate HRSAMs against previous methods, i.e., RITM [37], FocalClick [8], SimpleClick [56], InterFormer [31], SegNext [55], SAM [36], MobileSAM [104] and EfficientSAM [91]. For non-SAM models, we use their default input sizes. For SAM series models, we use both  $1024^2$  and  $2048^2$  inputs if the model supports  $2048^2$  inputs. In testing, click simulation places clicks at the centers of erroneously predicted regions, with the binary label of each click determined by the maximum distance to the boundaries of false negative and false positive regions, aligning with the previous methods [8, 56, 31]. We assess all models’ segmentation performance and speed. Segmentation performance is measured using 5-mIoU and NoC metrics. The 5-mIoU represents the average IoU after the fifth click. The NoC metric indicates the average minimum clicks required to reach a specified IoU. We focus on NoC@90 and NoC@95 within 20 clicks. Speed is quantified as Seconds Per Click (SPC) on GPUs, measuring the average inference latency per click, averaged over 20 clicks. For SAM series models, this includes the preprocessing time by the backbone.